

TD-DFT Analysis of the Dissymmetry Factor in Camphor

Iran da L. Sousa,^a Gabriel Heerd,^b Valdecir F. Ximenes,^c Aginaldo R. de Souza^c and Nelson H. Morgon^{✉*,a}^aInstituto de Química, Universidade Estadual de Campinas, 13083-861 Campinas-SP, Brazil^bDepartamento de Química, Universidade Federal de Minas Gerais, 31270-901 Belo Horizonte-MG, Brazil^cFaculdade de Ciências, Universidade Estadual Paulista, 17033-360 Bauru-SP, Brazil

The fact that the dissymmetry factor (g-factor) of camphor is large has been known for decades, and the interpretation of the observed data has also been known for a long time. However, due to the ability of quantum chemical methods to describe chiroptical phenomena more appropriately, additional approaches based on these methods have been successfully employed. The g-factor present in *S*-camphor and *L*-tryptophan have been investigated by UV-Vis and electronic circular dichroism (ECD) spectroscopies of the $n \rightarrow \pi^*$ electronic transition. Time-dependent density functional theory (TD-DFT) calculations at CAM-B3LYP/6-311++G(3df,2p)//B3LYP/6-311++G(2d,p) level of theory including Grimme's dispersion effects have been performed. The solvent effect was added using solvation model based on density (SMD) approach in solvation environment. The results permit insights into the ground and excited states electronic properties associated with the g-factor. The theoretical spectra showed good similarity with the experimental ones. The theoretical ECD of camphor was found at 282 nm, whereas the experimental shows its maximum at 290 nm. Regarding the maximum value of the molar absorptivity coefficient, the theoretical and experimental values were 16.2 and 30.2 M⁻¹ cm⁻¹, respectively. The same concordance was obtained for g-factor, as follows: -0.0445 and -0.0886, for experimental and theoretical results, respectively.

Keywords: *S*-camphor, *L*-tryptophan, UV-Vis, ECD, g-factor, TD-DFT

Introduction

This work has its background in the *ab initio* calculation of the UV-Vis absorption and electronic circular dichroism (ECD) spectra for camphor as have been commonly used, such as optical rotatory dispersion (ORD) and ECD spectroscopy.¹⁻⁵

ECD is a chiroptical spectroscopic technique based on differential absorption by a chiral molecule of left (A_l) and right (A_r) circularly polarized light in the UV and visible regions (equation 1). In this equation, ϵ_l and ϵ_r are the molar absorptivity coefficients for the left and right circularly polarized light, respectively, c is the molar concentration and b the path length.⁶

$$\text{ECD} = A_l - A_r = \epsilon_l - \epsilon_r = \Delta\epsilon (c b) \quad (1)$$

ECD is an extremely powerful method for exploration

of chirality and stereoselectivity of organic molecules and small biomolecules. The method is powerful source for structural information of proteins and can be used for understanding docking ligands into protein active sites.⁷⁻⁹

Of relevance in this work is the dissymmetry factor (g-factor), which is the ratio between the sample's ECD and absorbance values (equation 2).¹⁰ Differently of ECD or absorbance properties, the g-factor is independent of concentration and path length, i.e., it is an intensive property of a chiral compound. As such, g-factor spectra have been applied for the estimation of the secondary structures of proteins where the concentration and path length cannot be determined.¹¹ Other application of the g-factor included the determination of enantiomeric excess in mixture of enantiomers. This has particular relevance in photochirogenesis, a science that studies both the preferential predominance of one enantiomeric form in biomolecules and provides an understanding of the presence of excess amounts of *L*-amino acids in carbonaceous chondritic meteorites.¹² In addition, the analysis of g-factor can improve the reliability

*e-mail: nhmorgon@unicamp.br

of the absolute configuration assignments and to help in the discrimination among multiple diastereomers, how described by Polavarapu and co-workers.^{13,14}

$$g = \frac{A_l - A_r}{A} = \frac{\Delta\epsilon}{\epsilon} \quad (2)$$

Thus, unlike the use of the octant rule, this work is based on a time-dependent density functional theory (TD-DFT) explanation for the exceptionally high *g*-factor of camphor when compared to most of the others chiral molecules as amino acids, proteins and pharmaceutical drugs. Also, the *g*-factor of other molecular systems (L-tryptophan, *S*-naproxen, (+)-menthone, and *R*-3,3'-dibromo-1,1'-bi-2-naphthol) has been obtained from experimental and theoretical calculations for comparison.

Experimental

Experimental studies

S-Camphor, L-tryptophan, *S*-naproxen, (+)-menthone, and *R*-3,3'-dibromo-1,1'-bi-2-naphthol were purchased from Sigma-Aldrich Chemical Co. (St. Louis, MO, USA). Stock solutions of the compounds (10 mmol L⁻¹) were prepared in ethyl alcohol. CD and UV-Vis absorption studies were performed using a Jasco J-815 spectropolarimeter (Jasco, Japan) equipped with a thermostatically controlled cell holder. The spectra were obtained with 1 nm step resolution, response time of 1 s and scanning speed of 50 nm min⁻¹. A 3 mL quartz cuvette with a 10 mm path length and a magnetic stirrer were used for the measurements. The final concentrations of the studied compounds were: 1.75 mmol L⁻¹ *S*-camphor, 30 μmol L⁻¹ L-tryptophan, 15 μmol L⁻¹ *S*-naproxen and 30 μmol L⁻¹ *R*-3,3'-dibromo-1,1'-bi-2-naphthol. The baseline (ethyl alcohol) was subtracted from all measurements.

Quantum chemical calculations

Our studies started by a ground-state structure optimization based on density functional theory. The calculations were carried out using the exchange-correlation functional B3LYP and the molecules of interest were fully optimized without any constraints. The root mean square (RMS) force and displacements criteria of 1 × 10⁻⁶ were used during the molecular geometry optimization process. TD-DFT calculations were carried out considering the minimum energy configuration of the ground-state structure, using the CAM-B3LYP functional and Grimme's GD3-BJ dispersion effect. The triple-zeta Pople basis

sets, 6-311++G(2d,p) and 6-311++G(3df,2p), were used to represent the carbon, oxygen, nitrogen and hydrogen atoms. The first basis set was employed in the optimization processes, and the second one to single-point energy calculations. Ethanol (ε = 24.852) was used as solvent and its effect introduced in all the calculations through the SMD (solvent model density) approach. To simulate the UV-Vis and ECD spectrum 15 singlet-singlet transition states were considered. All computer simulations were done in the GridUNESP supercomputer facilities, which are composed of 3104 processing cores with a capacity of 77 TeraFlops. The storage capacity of these systems is 288 TB through DAS optical fiber (StorageTek 6140) and 96 TB at four SUN X4500 servers. All calculations were carried out using the Gaussian 09 suite of programs (revision D1).¹⁵

Results and Discussion

Molecular geometries

Camphor (1,7,7-trimethylbicyclo[2.2.1]heptan-2-one) is a well-known bicyclic terpenoid derived from the wood of the camphor laurel (*Cinnamomum camphora* tree). This chiral bicyclic ketone occurs naturally as the *R*-enantiomer.¹⁶ A long history of its use, especially in medicine, is reported in literature.¹⁷ Recently, several works are contributing to its description and properties analyses.¹⁸⁻²² In this work we have studied the electronic and molecular properties of the *S*-enantiomer (Figure 1a) and, for comparative purpose, of the L-tryptophan (Figure 1b).

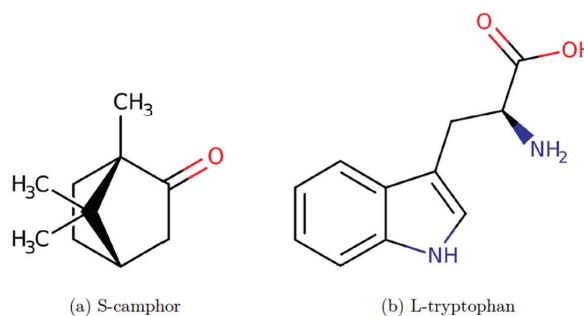


Figure 1. Molecular structures of (a) *S*-camphor and (b) L-tryptophan.

In case where there are several conformers which appear to be stable in terms of energy, as L-tryptophan (Figure 1b), ECD calculations generally involve two steps: first the conformational analysis of the compound to obtain the most relevant conformational structures, weighted considering the Boltzmann distribution law (equation 3).

$$P_i(\%) = \frac{e^{-\Delta(E_i)/RT}}{\sum_{i=1}^N e^{-\Delta(E_i)/RT}} \quad (3)$$

where P_i and E_i are the fractional population and energy of the i^{th} conformer at 298.15 K of temperature. And the second step involves the UV-Vis/ECD TD-DFT calculation of each conformer, selected in the previous one.

The conformational search, employed for finding the stable conformers, was performed by varying selected dihedral angles, as described at Supplementary Information (SI) section. The stable molecular geometries, corresponding to the energy minima on potential energy surface (PES), were obtained at the B3LYP/6-311++G(2d,p) level of theory.

Electronic circular dichroism

Theoretical ECD spectra were obtained by calculations of vertical excitation energies and rotatory strengths for the first 15 excited states. The calculated rotatory strengths from

these 15 singlet electronic transitions were simulated into an ECD curve using Gaussian band shapes with half-width at 0.6 eV. Figures 2 and 3 show the absorbance and ECD experimental and theoretical spectra of *S*-camphor (CAM) and *L*-tryptophan (TRY), respectively. For comparison purposes, the molar absorptivity coefficient for all systems studied, i.e., quantities related to the UV-Vis and ECD spectra intensities, are given at Table 1.

As should be expected due to the symmetry forbidden $n \rightarrow \pi^*$ transition in ketones, camphor has extremely low capacity of UV absorption (Figure 2). In the maximum absorption wavelength (296 nm), the molar absorptivity coefficient was obtained as $30.2 \text{ M}^{-1} \text{ cm}^{-1}$. This value is of the same magnitude as compared to aliphatic ketones.²³

This table shows that the molar absorptivity coefficient of *L*-tryptophan at 282 nm is $6.8 \times 10^3 \text{ M}^{-1} \text{ cm}^{-1}$, i.e., around

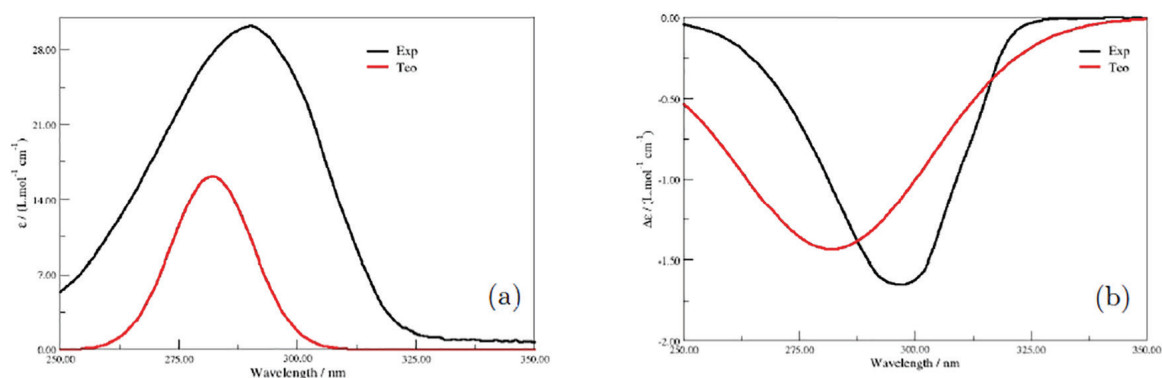


Figure 2. Experimental and theoretical (a) UV-Vis absorbance and (b) ECD spectra of *S*-camphor.

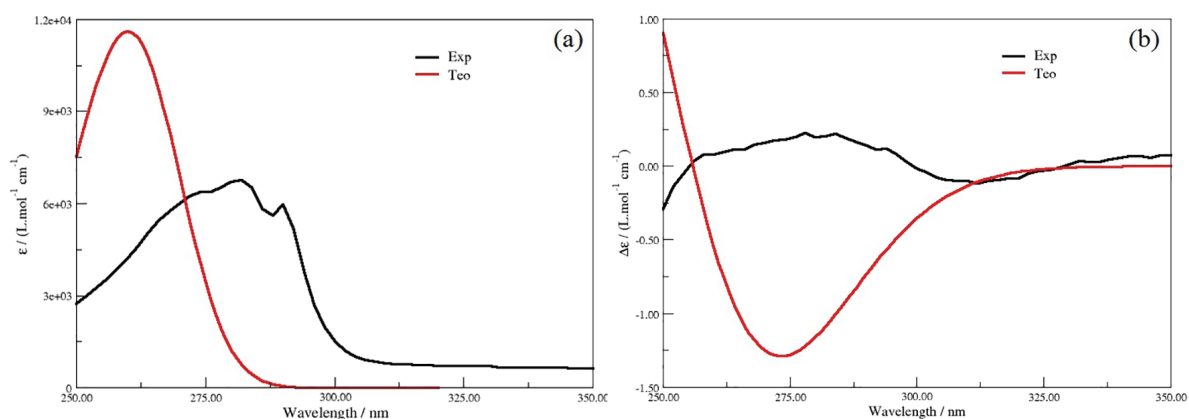


Figure 3. Experimental and theoretical (a) UV-Vis absorbance and (b) ECD spectra of *L*-tryptophan.

Table 1. Maximum absorption, λ_{max} , molar absorptivity coefficient, ϵ , molar circular dichroism, $\Delta\epsilon$, and g -factor for *S*-camphor and *L*-tryptophan. All of these quantities are related to the UV-Vis and ECD spectra intensities

Molecule	$\lambda_{\text{max}} / \text{nm}$	$\epsilon / (\text{M}^{-1} \text{ cm}^{-1})$	$\Delta\epsilon / (\text{M}^{-1} \text{ cm}^{-1})$	g
<i>S</i> -Camphor	282.0 (290.0) ^a	16.2 (30.2)	-1.44 (-1.51)	-0.0886 (-0.0445)
<i>L</i> -Tryptophan	263.0 (282.0)	11,609.0 (6,779.3)	-0.55 (0.41)	-0.0001 (0.0001)

^aThe experimental values are between parentheses.

10^3 -fold higher compared to *S*-camphor. Obviously, this is not unexpected, since this absorption band is related to an allowed $\pi \rightarrow \pi^*$ electronic transition.²³ However, despite the extremely low capacity of light absorption, the ECD intensity of *S*-camphor was of the same magnitude when compared to L-tryptophan. The fact that the *g*-factor of camphor is large has been known for decades, and the interpretation of the observed data has also been known for a long time. It has indeed been the basis of the celebrated octant rule proposed by Moscovitz²⁴ and the more recent by Lightner and Gurst.²⁵ In our work we have studied this unusual spectroscopic feature of *S*-camphor by visualization of its *g*-factor spectrum. This spectrum was obtained using TD-DFT and SMD levels of theory. The results at Table 1 and Figure 4 show that, at its maximum intensity wavelengths, the *g*-factor of *S*-camphor was around 800-fold higher compared to L-tryptophan. Specifically, the *g*-factors at their maximum were -0.0886 and -0.0001 for *S*-camphor and L-tryptophan, respectively.

To reinforce that *g*-factors usually have low values, we also measured, for comparative purpose, the *g*-factor of *S*-naproxen ($g = -0.0003$) and *R*-3,3'-dibromo-1,1'-bi-2-naphthol ($g = 0.0001$). These values are in agreement with most of the published results. For instance, in proteins, values around -0.005 are usually reported.¹¹ For amino acids values as 0.007 (L-alanine) and 0.008 (L-glutamic acid) were reported.²⁶ Looking for an explanation for this unusual spectroscopic property of *S*-camphor, *ab initio* calculations were performed to simulate its UV-Vis and ECD spectra and, for comparative purposes, regarding the value of *g*-factors, the same procedure was also studied. It is worth to remember that the efficiency of UV-Vis absorption, measured by the molar absorptivity coefficient (ϵ), is related to the theoretical quantity: oscillator strength (f), which is related to the transition electric dipole moment ($\vec{\mu}_{0,i}$), defined as follows in equations 4 and 5. The theoretical determination of the oscillator strength

between two bound states, Ψ_0 with energy E_0 and Ψ_i with energy E_i , involves the calculation with two wave functions and with the operator transition electric dipole moment ($\hat{\mu}$).⁶

$$f_{0 \rightarrow i} \propto \left[\int \Psi_0(\vec{r}) \hat{\mu} \Psi_i(\vec{r}) d\vec{r} \right]^2 \quad (4)$$

The relation between the dipole strength D_i and the oscillator strengths f_i , for each electronic transition, is given by the following equation.

$$f_i = \frac{8\pi^2 \tilde{\nu}_i m_e c}{3h e^2} D_i \quad (5)$$

where f_i is the (quantity dimensionless) oscillator strength corresponding to the electronic excitation of interest and D_i is the corresponding dipole strength; $\tilde{\nu}$ is the corresponding excitation energy in wavenumbers. The other constants are the charge of the electron (e) and electron mass (m_e), and h is the Planck constant. The simulated UV-Vis spectrum was obtained as the combination of the bands computed through TD-DFT calculations, employing 15 singlet-singlet transition states, with half-width at 0.6 eV. On the other hand, the ECD signal intensity is theoretically related to the rotatory strength quantity (R), which is related to the intensity of an absorption band from λ_1 to λ_2 (in cgs units) (equation 6):

$$R = 2.297 \times 10^{-39} \int_{\lambda_1}^{\lambda_2} \frac{\Delta\epsilon(\lambda)}{\lambda} d\lambda \quad (6)$$

The transition between Ψ_0 and Ψ_i states can be theoretically defined by equation 7, where $\hat{\mu}$ and \hat{m} are the electric and magnetic dipole operators, respectively. The electric and magnetic transition dipole moments $\vec{\mu}_{0,i}$ and $\vec{m}_{0,i}$, as well as the angle between both moments, have to be determined to obtain the theoretical ECD spectra and to perform a comparison with the experimental data.^{27,28} From equation 7 we can observe that the sign of the rotational

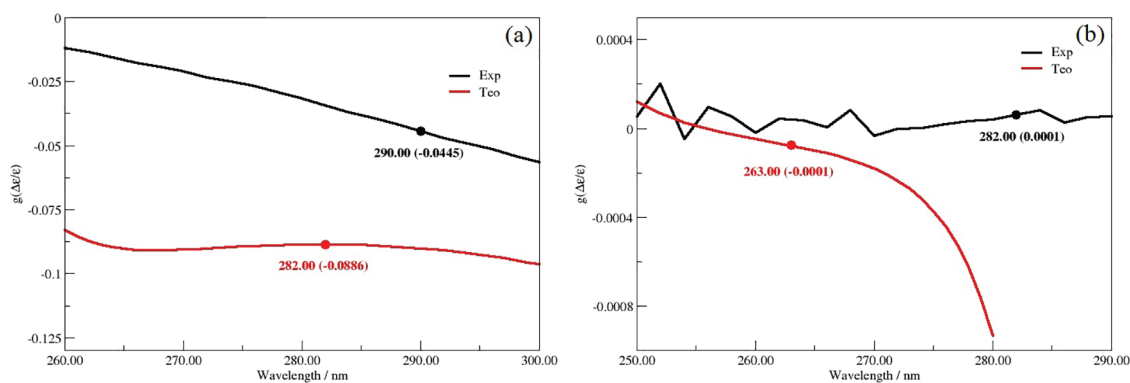


Figure 4. Experimental and theoretical *g*-factors of (a) *S*-camphor (CAM) and (b) L-tryptophan (TRY).

Table 2. Electronic parameters calculated for *S*-camphor and *L*-tryptophan molecules:^a transition electric dipole moment, μ_{ele} , transition magnetic dipole moment, μ_{mag} , oscillator strength, angle between the electric (E) and magnetic (M) transition dipole moments, and cosine of this angle. All of these quantities are related to the UV-Vis and ECD spectra intensities

Molecule	μ_{ele}	μ_{mag}	Intensity	E-M angle / degree	cos(E-M)
<i>S</i> -Camphor	0.0587	1.1830	0.0004	104.89	-0.257
<i>L</i> -Tryptophan	1.8241	0.9463	0.2107	90.54	-0.009

^aFor *L*-tryptophan, the calculated intensity are weighted considering the Boltzmann distribution law.

strength is determined by the angle between the electric and magnetic dipole transition moments [$\cos(\vec{\mu}_{0,i}, \vec{m}_{0,i})$]. The rotational strength is given by equation 7:

$$R_{0,i} = \Im(\mu_{0,i} \cdot m_{0,i}) \quad (7)$$

where $\mu_{0,i} = \int \Psi_f^*(q) \hat{\mu} \Psi_i(q) d\tau$ and $m_{0,i} = \int \Psi_f^*(q) \hat{m} \Psi_i(q) d\tau$, i.e., the imaginary component of the scalar product between the electric and magnetic moments. For most purposes, we can say that $R_{0,i}$ can be described by $|\vec{\mu}_{0,i}| |\vec{m}_{0,i}| \cos(\vec{\mu}_{0,i}, \vec{m}_{0,i})$, where $\cos(\vec{\mu}_{0,i}, \vec{m}_{0,i})$ is the angle between these two dipoles.

As can be observed at Table 1, the theoretical spectra showed good similarity with the experimental results. In the case of the camphor molecule, the maximum of the theoretical ECD was obtained at 282 nm, whereas the experimental result was equal to 290 nm. Regarding the molar absorptivity coefficient, at its maximum, the theoretical and experimental values were 16.2 and 30.2 $\text{M}^{-1} \text{cm}^{-1}$, respectively. The same concordance was obtained for *L*-tryptophan. Once obtained excellent matches between experimental and theoretical spectra, the next step was to search out for an explanation for the relatively high *g*-factor of camphor. To this end, the magnitude and the angle between the electric and magnetic transition dipole moments were calculated at their maximum wavelengths.

It is worth to note that the light absorption depends only on the electric transition dipole moments (equation 5). Hence, as expected, the magnitude of electric component for *S*-camphor was lower as compared to *L*-tryptophan, which is in agreement with its lower molar absorptivity coefficient (Table 2).

On the other side, the opposite was obtained in relation to the magnetic component. Hence, taking into account that the intensity of rotational strength is given by the scalar product of the vectors (equation 7), we propose that the higher magnitude of the magnetic component could compensate the lower value of the electric one, leading to ECD signal intensity similar to that obtained for tryptophan. The magnitude of the ECD spectra signs for *S*-camphor and *L*-tryptophan can also be explained by the angle between these two vectors. For the angle value equal to 104.89°,

we obtain $\cos(\text{E-M}) = -0.257$, and for 90.54°, the angle is $\cos(\text{E-M}) = -0.009$.

Conclusions

As a quotient ($\Delta\epsilon/\epsilon$) (equation 2), the high *g*-factor value for camphor is the consequence of the low value of ϵ in this symmetry forbidden transition. Interestingly, the inefficient electronic transition (related to the theoretical parameter electronic transition dipole moment) was not followed by a low ECD value ($\Delta\epsilon$), which is related to both electronic and magnetic transition dipole moments. Two factors explain this finding: (i) the magnetic transition dipole moment does not follow its electronic counterpart and presented a relatively high value in camphor; indeed, much higher compared to tryptophan; (ii) the angles between these vector quantities also favored camphor (Table 1). As the rotatory strength (*R*) is a dot product of electronic and magnetic transition dipole moments, the low value of the former was compensated by the last and the angle between them. These findings could be used as a didactic exemplification of the connection between vector algebra and molecular properties.

Supplementary Information

Supplementary data (molecular geometries, electronic energies and the fractional populations of all systems and conformers described in this work) are available free of charge at <http://jbcs.sbcq.org.br> as PDF file.

Acknowledgments

This work was supported by the Foundation of the State of São Paulo (FAPESP, grants 2016/20549-5, 2015/22338-9, 2016/308480-3, 2016/04963-6, 2019/12294-5) and INCT. Bio.Nat (2014/50926-0), National Council for Scientific and Technological Development (CNPq, grants 302793/2016-0, 306975/2013-0, 305541/2017-0 and 440503/2014-0). This research was supported by resources supplied by the Center for Scientific Computing (NCC/GridUNESP) of the São Paulo State University (UNESP).

References

1. Autschbach, J.; Jensen, L.; Schatz, G. C.; Tse, Y. C. E.; Krykunov, M.; *J. Phys. Chem. A* **2006**, *110*, 2461.
2. Rossi, S.; Nostro, P. L.; Lagi, M.; Ninham, B. W.; Baglioni, P.; *J. Phys. Chem. B* **2007**, *111*, 10510.
3. Ximenes, V. F.; Morgon, N. H.; de Souza, A. R.; *Chirality* **2018**, *30*, 1049.
4. Shubert, V. A.; Schmitz, D.; Schnell, M.; *J. Mol. Spectrosc.* **2014**, *300*, 31.
5. de Souza, A. R.; Ximenes, V. F.; Morgon, N. H. In *Stereochemistry and Global Connectivity: The Legacy of Ernest L. Eliel*, vol. 2; Cheng, H. N.; Maryanoff, C. A.; Miller, B. D.; Schmidt, D. G., eds.; American Chemical Society: New York, 2017, p. 91-101.
6. Warnke, I.; Furche, F.; *WIREs Comput. Mol. Sci.* **2012**, *2*, 150.
7. Costa, E. V.; da Cruz, P. E. O.; Pinheiro, M. L. B.; Marques, F. A.; Ruiz, A. L. T. G.; Marchetti, G. M.; de Carvalho, J. E.; Barison, A.; Maia, B. H. L. N. S.; *J. Braz. Chem. Soc.* **2013**, *24*, 788.
8. Chaves, O. A.; Soares, B. A.; Maciel, M. A. M.; Sant'Anna, C. M. R.; Netto-Ferreira, J. C.; Cesarin-Sobrinho, D.; Ferreira, A. B. B.; *J. Braz. Chem. Soc.* **2016**, *27*, 1858.
9. Chaves, O. A.; Ferreira, R. C.; da Silva, L. S.; de Souza, B. C. E.; Cesarin-Sobrinho, D.; Netto-Ferreira, J. C.; Sant'Anna, C. M. R.; Ferreira, A. B. B.; *J. Braz. Chem. Soc.* **2018**, *29*, 1551.
10. Wakabayashi, M.; Yokojima, S.; Fukaminato, T.; Shiino, K.; Irie, M.; Nakamura, S.; *J. Phys. Chem. A* **2014**, *118*, 5046.
11. McPhie, P.; *Anal. Biochem.* **2001**, *293*, 109.
12. Bredehöft, J. H.; Jones, N. C.; Meinert, C.; Evans, A. C.; Hoffmann, S. V.; Meierhenrich, U. J.; *Chirality* **2014**, *26*, 373.
13. Polavarapu, P. L.; *Molecules* **2016**, *21*, 1055.
14. Johnson, J. L.; Nair, D. S.; Pillai, S. M.; Johnson, D.; Kallingathodii, Z.; Ibnusaud, I.; Polavarapu, P. L.; *ACS Omega* **2019**, *4*, 6154.
15. Frisch, M. J.; Trucks, G. W.; Schlegel, H. B.; Scuseria, G. E.; Robb, M. A.; Cheeseman, J. R.; Scalmani, G.; Barone, V.; Mennucci, B.; Petersson, G. A.; Nakatsuji, H.; Caricato, M.; Li, X.; Hratchian, H. P.; Izmaylov, A. F.; Bloino, J.; Zheng, G.; Sonnenberg, J. L.; Hada, M.; Ehara, M.; Toyota, K.; Fukuda, R.; Hasegawa, J.; Ishida, M.; Nakajima, T.; Honda, Y.; Kitao, O.; Nakai, H.; Vreven, T.; Montgomery Jr., J. A.; Peralta, J. E.; Ogliaro, F.; Bearpark, M.; Heyd, J. J.; Brothers, E.; Kudin, K. N.; Staroverov, V. N.; Kobayashi, R.; Normand, J.; Raghavachari, K.; Rendell, A.; Burant, J. C.; Iyengar, S. S.; Tomasi, J.; Cossi, M.; Rega, N.; Millam, N. J.; Klene, M.; Knox, J. E.; Cross, J. B.; Bakken, V.; Adamo, C.; Jaramillo, J.; Gomperts, R.; Stratmann, R. E.; Yazyev, O.; Austin, A. J.; Cammi, R.; Pomelli, C.; Ochterski, J. W.; Martin, R. L.; Morokuma, K.; Zakrzewski, V. G.; Voth, G.; Salvador, P.; Dannenberg, J. J.; Dapprich, S.; Daniels, A. D.; Farkas, Ö.; Foresman, J. B.; Ortiz, J. V.; Cioslowski, J.; Fox, D. J.; *Gaussian 09, Revision D.1*, Gaussian, Inc., Wallingford, CT, 2009.
16. Rautenstrauch, V.; Lindström, M.; Bourdin, B.; Currie, J.; Oliveros, E.; *Helv. Chim. Acta* **1993**, *76*, 607.
17. Hamidpour, R.; Hamidpour, S.; Hamidpour, M.; Shahlari, M.; *Int. J. Case Rep. Imag.* **2013**, *4*, 86.
18. Rietveld, I. B.; Barrio, M.; Veglio, N.; Espeau, P.; Tamarit, J. L.; Céolin, R.; *Thermochim. Acta* **2010**, *511*, 43.
19. Andersson, O.; Ross, R. G.; Jezowski, A.; *Mol. Phys.* **1990**, *70*, 1065.
20. Kisiel, Z.; Desyatnyk, O.; Białkowska-Jaworska, E.; Pszczółkowski, L.; *Phys. Chem. Chem. Phys.* **2003**, *5*, 820.
21. Kokkinou, A.; Tsorteki, F.; Karpusas, M.; Papakyriakou, A.; Bethanis, K.; Mentzafos, D.; *Carbohydr. Res.* **2010**, *345*, 1034.
22. Brunelli, M.; Fitchci, A. N.; Mora, A. J.; *J. Solid State Chem.* **2002**, *163*, 253.
23. Turro, N.; *Modern Molecular Photochemistry*; University Science Books: Mill Valley, CA, 1991.
24. Moskowitz, A.; *Optical Rotatory Dispersion*; Djerassi, C., ed.; McGraw-Hill: New York, 1960.
25. Lightner, D.; Gurst, J. E.; *Organic Conformational Analysis and Stereochemistry from Circular Dichroism Spectroscopy*; Wiley-VCH: New York, 2000.
26. Meierhenrich, U.; *Amino Acids and the Asymmetry of Life: Caught in the Act of Formation*; Springer: Berlin, 2008.
27. Diedrich, C.; Grimme, S.; *J. Phys. Chem. A* **2003**, *107*, 2524.
28. Honda, Y.; Kurihara, A.; Kenmochi, Y.; Hada, M.; *Molecules* **2010**, *15*, 2357.

Submitted: June 17, 2019

Published online: September 20, 2019

